Skyrmion–anti-Skyrmion annihilation with ω mesons

M. Á. Halász and R. D. Amado
Department of Physics and Astronomy, University of Pennsylvania, Philadelphia, Pennsylvania 19104-6396
(Received 21 September 2000; published 7 February 2001)

We study numerically the annihilation of an ω-stabilized Skyrmion and an anti-Skyrmion in three spatial dimensions. To our knowledge this is the first successful simulation of Skyrmion–anti-Skyrmion annihilation which follows through to the point where the energy is carried by outgoing meson waves. We encounter instabilities similar to those encountered is earlier calculations, but in our case these are not fatal and we are able to simulate through this process with a global energy loss of less than 8% and to identify robust features of the final radiation pattern. The system passes through a singular configuration at the time of half-annihilation. This is followed by the onset of fast oscillations which are superimposed on the smoother process which leads to the appearance of outgoing waves peaked at roughly 45° to the incident direction. We investigate the two prominent features of this process: the proliferation of small, fast oscillations and the singular intermediate configuration. We find that our equations of motion allow for a regime in which the amplitude of certain small perturbations increases exponentially. This regime is similar but not identical to the situation pointed out earlier regarding the original Skyrme model. We argue that the singularity may be seen as the result of a pinch effect similar to that encountered in plasmas.

DOI: 10.1103/PhysRevD.63.054020 PACS number(s): 12.39.Dc, 11.10.Lm, 13.75.Cs

I. INTRODUCTION

The attractive idea of representing nucleons as solitons of the effective pion field was proposed by Skyrme long before the advent of QCD [1]. In the context of QCD, the idea remains equally attractive; moreover, the approach becomes exact in the large N_c limit [2]. The Skyrme approach gives a classical, nonperturbative picture of hadrons in the context of low-energy QCD. Many properties of nucleons are reobtained using a model of quantized spinning solitons of the pion field [3], including the static nucleon-nucleon and nucleon-antinucleon [4] potentials.

The main difficulty in using the Skyrme approach as a starting point for an effective dynamical theory of nucleons lies in the fact that all such enterprises must use numerical calculations to describe the dynamics of the solitons. No analytic solutions are known. One path is to study the classical dynamics of Skyrmions and use the results to build up the quantum dynamics of nucleons based on the model of the static nucleon as a superposition of spinning Skyrmions. Conceptually the simplest process one might study this way is low-energy nucleon-antinucleon annihilation since in this case there are no nucleons in the final state. At low energies the initial state is reasonably well described by Skyrmions, while in the final state there are only mesons which again are well described by the effective theory [5].

Simulating soliton-antisoliton annihilation has proved to be a difficult numerical problem. Previous attempts to simulate the annihilation of a Skyrmion–anti-Skyrmion pair [6–8] using the original Skyrme Lagrangian encountered numerical difficulties. The problem has been [7] traced to a deviation from the hyperbolic nature of the equations of motion, resulting from the contact nature of the Skyrme term. Another possible concern is that the low-energy approximation becomes questionable during the annihilation process when the energy tied up in the solitons is suddenly liberated. Notwithstanding, below we present the first successful attempt at such a simulation using omega stabilization instead of the Skyrme term. We are able to follow the Skyrmions from incidence through annihilation to pion radiation. An interesting phenomenon involving a possible pointlike singularity arises in our calculation that might actually simplify the analysis; however, our objective for now is to obtain a base line calculation using classical Skyrmion dynamics. We will return to a detailed discussion of the singularities in a subsequent publication.

In this paper we present our results on Skyrmion–anti-Skyrmion annihilation using a model [9–11] which couples a U(1) vector field (the ω) to the winding number of the SU(2) (pion) field. This coupling replaces the Skyrme term for stabilizing the Skyrmion. The idea of replacing the highly nonlinear Skyrme term with a coupling to additional vector fields, in particular to the ω, goes back to Adkins and Nappi [11]. It has been widely used in studies of the Skyrme model (see [3] for more details). The configuration of the pion field in the static hedgehog Skyrmion is similar to the traditional one. The ω field in this case has only an ω_0 component. Numerical studies of the static interaction of such Skyrmions [4] have been performed earlier. We have studied the classical scattering of two such Skyrmions [9] for a variety of relative groomings and impact parameters, and found that the corresponding dynamics is very similar to that of traditional Skyrmions. The omega stabilization is gentler than the Skyrme term and should thus lead to less violent behavior in the simulations. We are able to follow through the annihilation process to the point when the energy is carried by outgoing spherical (pion and ω) waves. We encountered significant, but not fatal, numerical difficulties, and could ensure energy conservation to better than 8%. Our programs are set up for general initial conditions, and we will investigate the dependence on those separately. The results we present below refer only to the head-on annihilation process with fixed initial velocity. To our knowledge the annihilation process has not been followed this far previously.

The annihilation itself, in the sense of the unwinding of

 ©2001 The American Physical Society

the baryon number, takes place in a time comparable to the size of the Skyrmions. It proceeds through an intermediary state which has a pointlike singularity, which results in the concentration of the total energy in a very small region around the symmetry center. This is followed by fast oscillations which last for a time comparable to the unwinding, and then gradually give way to outgoing (quasi)spherical waves which are suppressed at small angles and peak around 45°.

For the original Skyrme model, the Skyrme term was identified as the source of numerical instability [7]. Our effective Lagrangian does not have a similar local self-interaction term for the pion field. However, we have encountered numerical problems similar to those expected when the equations are no longer purely hyperbolic—namely, the appearance of persistent fast oscillations of small amplitude which make the simulation difficult. After a more careful analysis, we found that our equations of motion also allow for nonhyperbolic solutions (i.e., plane waves with imaginary wave number) albeit at a higher order than the Skyrme equations. Fortunately, in our case these oscillations are weak enough so as to not completely destroy the long-wavelength features. Thus our central results seem to be robust and independent of the violent short-wavelength behavior.

The most prominent feature of the annihilation process, and probably the ultimate source of our numerical difficulties, is the fact that close to the point of half-annihilation, when the original tips of the Skyrmion and the anti-Skyrmion merge, the pion field has a singular configuration. The fields themselves are continuous, but the derivatives are singular. We do not yet have a complete, quantitative understanding of this phenomenon, but it is clear that it consists of the axial baryon current (which carries out the annihilation) being squeezed into a very small, probably pointlike cross section. This feature is localized in the $x=0$ symmetry plane (the one that separates the Skyrmion and the anti-Skyrmion), and arises close to the moment of half-annihilation.

In the following section we define our model Lagrangian and derive the equations of motion. The main part of this paper is contained in Sec. III, where we describe our numerical results on the phenomenology of axial-symmetric annihilation and discuss our simulation. The first part of this section describes our calculation, with emphasis on aspects not already discussed in [9]. The reader interested only in the phenomenology of the annihilation may skip directly to Sec. III B and omit Sec. III C where we present numerical checks to assess the reliability of our results. In Sec. IV we investigate the stability of our equations of motion against small plane-wave-like perturbations, in the spirit of [7], and attempt to identify signs of nonhyperbolicity in our results. In Sec. V we discuss the appearance of a singularity in the pion field at the moment of half-annihilation. While we can understand qualitatively the mechanism that produces this phenomenon, a full understanding will require more focused investigation. In Sec. VI we summarize our results and make a wish list of further work. The Appendix contains a more detailed description of our numerical algorithm.

II. MODEL

Our Lagrangian consists of the nonlinear sigma model piece

$$\mathcal{L}_\sigma=\frac{1}{4}f_\pi^2\mathrm{tr}(\partial_\mu\mathcal{U}\partial^\mu\mathcal{U}^\dagger)+\frac{1}{2}m_\pi^2f_\pi^2\mathrm{tr}(\mathcal{U}-1) \tag{1}$$

and the omega piece

$$\mathcal{L}_\omega=-\frac{1}{2}\partial_\mu\omega_\nu(\partial^\mu\omega^\nu-\partial^\nu\omega^\mu)+\frac{1}{2}M^2\omega_\mu\omega^\mu, \tag{2}$$

which are coupled through the baryon current:

$$\mathcal{L}_{int}=\frac{3g}{2}\omega_\mu B^\mu,$$
$$B^\mu=\frac{1}{12\pi^2}\epsilon^{\mu\nu\alpha\beta}\mathrm{tr}[(\mathcal{U}^\dagger\partial_\nu\mathcal{U})(\mathcal{U}^\dagger\partial_\alpha\mathcal{U})(\mathcal{U}^\dagger\partial_\beta\mathcal{U})]. \tag{3}$$

The SU(2) field $\mathcal{U}$ is parametrized by the three real pion fields $\{\pi_k\}_{k=1,3}=\vec{\pi}$ or by the four ''Cartesian'' components $\mathbf{\Psi}=\{\Psi^A\}_{A=0,3}$:

$$\mathcal{U}=\exp(i\vec{\tau}\cdot\vec{\pi})=\Psi_0+i\vec{\tau}\cdot\vec{\Psi}=S^A\Psi^A\ (A=0,\ldots,3). \tag{4}$$

In our previous calculation we have used the π parametrization exclusively. For a detailed derivation of the equations of motion and a description of the corresponding numerical method we refer the reader to [9]. The more traditional method is to use the Ψ parametrization. That choice of variables has the advantage of being more transparent. Below we derive the equations of motion in the Ψ parametrization and describe a way to employ them in simulations without having to deal with Lagrange multipliers as dynamical variables. We used this approach to perform numerical calculations together with another code based on the π parametrization. The equations of motion below are crucial for the analysis presented in Sec. IV.

In the Ψ parametrization the baryon current is

$$B^\mu=\frac{1}{12\pi^2}\epsilon^{\mu\nu\alpha\beta}\epsilon^{ABCD}\Psi^A\partial_\nu\Psi^B\partial_\alpha\Psi^C\partial_\beta\Psi^D, \tag{5}$$

and the nonlinear σ piece is given by

$$\mathcal{L}_\sigma=\frac{1}{2}f_\pi^2\partial_\mu\Psi^A\partial^\mu\Psi^A+\frac{1}{2}m_\pi^2f_\pi^2(\Psi^0-1). \tag{6}$$

The Ψ^A's are subject to the chiral constraint which is equivalent to the unitarity condition on the $\mathcal{U}$'s:

$$\mathcal{U}\mathcal{U}^\dagger=\mathbf{1}\rightarrow\Psi^A\Psi^A=1. \tag{7}$$

To get meaningful equations of motion, we must impose this constraint separately on the components Ψ^A. One way is to introduce a Lagrange multiplier λ, adding a term $\lambda/2(\Psi^A\Psi^A-1)$ to the Lagrangian. The physical meaning of the multiplier is similar to that of ''reaction'' forces in me-

chanics, which enforce constraints without performing any work. Obviously, the equation of motion for λ is just the constraint equation (7), which now has to be solved along with the other equations of motion.

Our task is to solve formally the ordinary equations of motion for the dynamical variables and their derivatives. These will contain λ. Then, one uses the result and the constraint equation to solve for λ. Below, this will turn out to be straightforward.

To obtain the equations of motion for Ψ^A, start with the derivatives of $\mathcal{L}_\sigma+\mathcal{L}_\lambda$:

$$\frac{\delta(\mathcal{L}_\sigma+\mathcal{L}_\lambda)}{\delta(\Psi^A)}=m_\pi^2 f_\pi^2 \delta^{A0}\Psi^0+\lambda\Psi^A,$$

$$\frac{\delta(\mathcal{L}_\sigma+\mathcal{L}_\lambda)}{\delta(\partial_\mu\Psi^A)}=f_\pi^2\partial^\mu\Psi^A,\quad \partial_\mu\frac{\delta(\mathcal{L}_\sigma+\mathcal{L}_\lambda)}{\delta(\partial_\mu\Psi^A)}=f_\pi^2\partial_\mu\partial^\mu\Psi^A.$$

The derivatives of $\mathcal{L}_{int}$ are

$$\frac{\delta\mathcal{L}_{int}}{\delta(\Psi^A)}=\frac{g}{8\pi^2}\epsilon^{\mu\nu\alpha\beta}\omega_\mu\epsilon^{ABCD}\partial_\nu\Psi^B\partial_\alpha\Psi^C\partial_\beta\Psi^D,$$

$$\partial_\nu\frac{\delta\mathcal{L}_{int}}{\delta(\partial_\nu\Psi^B)}=\frac{3g}{8\pi^2}\{\epsilon^{\mu\nu\alpha\beta}\omega_\mu\epsilon^{ABCD}\partial_\nu\Psi^A\partial_\alpha\Psi^C\partial_\beta\Psi^D+\epsilon^{\mu\nu\alpha\beta}\partial_\nu\omega_\mu\epsilon^{ABCD}\Psi^A\partial_\alpha\Psi^C\partial_\beta\Psi^D\}.$$

The Ψ^A equation of motion is

$$f_\pi^2\partial_\mu\partial^\mu\Psi^A=\frac{3g}{8\pi^2}\epsilon^{\alpha\beta\mu\nu}\epsilon^{ABCD}\left\{\partial_\nu\omega_\mu\Psi^B\partial_\alpha\Psi^C\partial_\beta\Psi^D+\frac{4}{3}\omega_\mu\partial_\nu\Psi^B\partial_\alpha\Psi^C\partial_\beta\Psi^D\right\}+m_\pi^2 f_\pi^2\delta^{A0}\Psi^0+\lambda\Psi^A. \tag{8}$$

We can now proceed to eliminate λ. The chiral condition means that $\mathbf{\Psi}=\{\Psi^A\}$ is a four-dimensional unit vector. This leads to constraints of its derivatives. The first derivative of $\mathbf{\Psi}$ with respect to any one of the four coordinates must be perpendicular to $\mathbf{\Psi}$ and so on:

$$\Psi^A\Psi^A=1\rightarrow\partial_\mu\Psi^A\Psi^A=0\rightarrow\sum_A(\partial_\mu^2\Psi^A)\Psi^A+\sum_A(\partial\Psi^A)^2=0$$

or, after summing over μ,

$$\partial_\mu\partial^\mu\Psi^A\Psi^A+\partial_\mu\Psi^A\partial^\mu\Psi^A=0. \tag{9}$$

Geometrically this means that the component of $\partial_\mu\partial^\mu\mathbf{\Psi}$ parallel to $\mathbf{\Psi}$ is not a dynamical variable, but rather it is determined by the constraint. The corresponding part of the equation of motion (8) therefore carries no information about $\mathbf{\Psi}$. Instead, it tells us what λ should be in order to make sure Eq. (9) and thus Eq. (7) are verified.

Now we just project Eq. (8) onto $\mathbf{\Psi}$ and solve for λ:

$$\begin{aligned}\lambda&=f_\pi^2\Psi^A\partial_\mu\partial^\mu\Psi^A-\frac{g}{2\pi^2}\epsilon^{\mu\nu\alpha\beta}\epsilon^{ABCD}\omega_\mu\Psi^A\partial_\nu\Psi^B\partial_\alpha\Psi^C\partial_\alpha\Psi^D-m_\pi^2 f_\pi^2(\Psi^0)^2\\&=-f_\pi^2\partial_\mu\Psi^A\partial^\mu\Psi^A-\frac{g}{2\pi^2}\epsilon^{\mu\nu\alpha\beta}\epsilon^{ABCD}\omega_\mu\Psi^A\partial_\nu\Psi^B\partial_\alpha\Psi^C\partial_\alpha\Psi^D-m_\pi^2 f_\pi^2(\Psi^0)^2.\end{aligned} \tag{10}$$

From the second form it is clear that we have indeed solved for λ. Remember that we have a set of second-order partial differential equations. An initial condition specifies all the fields and their first derivatives, so the right-hand side of the second equation contains only known quantities. We can now replace this expression for λ into the full equation of motion.

One more observation is necessary. Since $\mathbf{\Psi}$ is a unit vector, all the $\partial_\mu\mathbf{\Psi}$'s are perpendicular to it. Consider the quantity

$$\epsilon^{\mu\nu\alpha\beta}\epsilon^{ABCD}\partial_\nu\Psi^B\partial_\alpha\Psi^C\partial_\beta\Psi^D. \tag{11}$$

Each nonzero term in the sum over Lorentz indices is perpendicular (in isospin space) to three distinct vectors $\partial_\nu\mathbf{\Psi}$, . . . , all of which are perpendicular to $\mathbf{\Psi}$. (Contracting with any of them would give zero because of the ϵ^{ABCD}.) Furthermore, the three vectors have to be linearly independent in order to give a nonzero contribution. But there are four mutually perpendicular directions altogether in this space; therefore the above quantity is necessarily parallel to $\mathbf{\Psi}$:

$$\epsilon^{\mu\nu\alpha\beta}\epsilon^{ABCD}\partial_\nu\Psi^B\partial_\alpha\Psi^C\partial_\beta\Psi^D=\Psi^A\epsilon^{\mu\nu\alpha\beta}\epsilon^{EBCD}\Psi^E\partial_\nu\Psi^B\partial_\alpha\Psi^C\partial_\beta\Psi^D. \tag{12}$$

Now we are ready to replace λ in the equation of motion, and we obtain

$$f_\pi^2\left[(\partial_\mu\partial^\mu\Psi^A-\Psi^A(\Psi^E\partial_\mu\partial^\mu\Psi^E)\right]=\frac{3g}{8\pi^2}\epsilon^{\alpha\beta\mu\nu}\epsilon^{ABCD}\partial_\nu\omega_\mu\Psi^B\partial_\alpha\Psi^C\partial_\beta\Psi^D+m_\pi^2 f_\pi^2\Psi^0(\delta^{A0}-\Psi^A\Psi^0). \tag{13}$$

The left-hand side is just the piece of $\partial_\mu\partial^\mu\mathbf{\Psi}$ which is perpendicular to $\mathbf{\Psi}$, $(\partial_\mu\partial^\mu\mathbf{\Psi})_\perp=\partial_\mu\partial^\mu\mathbf{\Psi}-\mathbf{\Psi}(\mathbf{\Psi}\cdot\partial_\mu\partial^\mu\mathbf{\Psi})$. So the equation of motion is written compactly:

$$(\partial_\mu \partial^\mu \Psi^A)_\perp - m_\pi^2 \Psi^0 (\delta^{A0} - \Psi^0 \Psi^A) = \frac{3g}{8 f_\pi^2 \pi^2} \epsilon^{\alpha\beta\mu\nu} \epsilon^{ABCD} \partial_\nu \omega_\mu \Psi^B \partial_\alpha \Psi^C \partial_\beta \Psi^D. \quad (14)$$

It is easy to derive the ω equation of motion

$$\partial^\nu \partial_\nu \omega^\mu = \partial^\mu \partial_\nu \omega^\nu - M^2 \omega^\mu + \frac{g}{8\pi^2} \epsilon^{\mu\nu\alpha\beta} \epsilon^{ABCD} \partial_\nu \Psi^A \Psi^B \partial_\alpha \Psi^C \partial_\beta \Psi^D. \quad (15)$$

This completes the set of equations of motion in the Ψ parametrization. They have the virtue of being more transparent than the ones based on the π fields.

III. NUMERICAL RESULTS

This section contains the central result of the paper. The reader interested only in the physics of annihilation as we understand it may skip the technical part of the first subsection and the third subsection in its entirety.

The purpose of the work reported here is to establish to which extent a numerical simulation of Skyrmion–anti-Skyrmion annihilation can be performed in the ω-stabilized model. We will see below that this simulation can indeed be performed successfully.

In the following subsection we describe our choice of parameters for the problem. These choices were driven by the fact that to our knowledge this is the first successful calculation that follows through the annihilation of a stable three-dimensional soliton and its antisoliton;[1] therefore our focus was on performing the most numerically accessible calculation which has the important qualitative features of the general case.

The second subsection contains a detailed description of the phenomenology of the central annihilation calculation. The annihilation proceeds through a sequence of very fast-varying intermediate configurations where most of the total energy is concentrated in a region of about half the linear size of one Skyrmion. This is followed by outgoing waves, which we followed for about 5 fm/c. Fast oscillations of small amplitude accompany the radiation phase.

The third subsection reports numerical checks on the reliability of our calculation. We compare results for the same calculation performed with different lattice spacings and show that while there are fluctuations, the macroscopic features, such as the time dependence of the energy flow and its angular distribution, are robust.

A. Simulation

The main challenge of this calculation lies in coping with the fast spatial and temporal variations of the field in the annihilation process. These require finer spatial grids and smaller time steps than smoother processes such as soliton scattering in order to avoid increasing numerical error which ultimately can make a calculation meaningless. Our choice of parameters is motivated by the desire to reduce this problem as much as possible.

We chose parameters close to those used in our previous work on scattering [9], but took a smaller mass for the vector field. This choice leads to a softer dynamics, but a dynamics which does not differ qualitatively from that for a physical mass. Our choice of parameters is therefore the same as in [9], with $f_\pi = 64$ MeV, $m_\pi = 139$ MeV, $g = m_\omega / f_\pi \sqrt{2}$, but $m_\omega = 385$ MeV. The Skyrmions in our case are slightly smaller in spatial size (1.1 fm versus 1.4 fm in diameter), and have a mass of 650 MeV.

We consider the special case of head-on annihilation. The original direction of motion is along the x axis. The Skyrmion and the anti-Skyrmion are located symmetrically on opposite sides of the $x=0$ plane, with their centers on the x axis. The Skyrmion is a standard hedgehog field configuration centered at $x=-1.5$ fm. The anti-Skyrmion is obtained by charge conjugating a hedgehog configuration centered at $x=1.5$ fm and then performing a grooming of 180° around the 1 or x axis: $(\Psi^0,\Psi^1,\Psi^2,\Psi^3) \to (\Psi^0,-\Psi^1,-\Psi^2,-\Psi^3) \to (\Psi^0,-\Psi^1,\Psi^2,\Psi^3)$—altogether, the anti-Skyrmion is obtained from the Skyrmion by changing the sign of the x or Ψ^1 component. This choice of grooming corresponds to the most attractive interaction between the Skyrmion and anti-Skyrmion.

The central annihilation problem has an additional axial symmetry compared to the general case. However, our codes take only partial advantage of the axial symmetry. We have full three-dimensional programs which we plan to use to perform a sweep of many initial conditions. We expect that most of the features of off-center annihilation (not head on) are encountered in the present setup, since the relative position and orientation of the solitons in the general case are very similar to those in central annihilation.

We performed simulations of Skyrmion–anti-Skyrmion annihilation using both the algorithm presented in [9] and a similar calculation based on the equations of motion from the previous section. Below and in the Appendix we describe the latter in more detail. The only major modification of the first calculation compared to [9] is the treatment of the ω field which is similar to that described below. The two calculations give virtually identical results in the smooth regime, with small differences in the violent regime. In the next subsection we present the results of a calculation using the Ψ scheme. The scaling analysis runs in Sec. III C use the π scheme. Since the Ψ scheme is more transparent, it is used for the study of the small oscillations and of the singularity in the respective sections.

One important modification compared to [9], which also affects the π scheme, refers to the implementation of the gauge fields. Taking the four-divergence of the ω equation of motion, together with baryon current conservation, leads to

$$M^2 \partial_\mu \omega^\mu = 0. \quad (16)$$

[1] A very interesting recent calculation of scattering of metastable baby Skyrmions [12] reported results on annihilation as well.

In other words, the nonzero mass breaks gauge symmetry, enforcing the Lorentz gauge. We can drop the $\partial^\nu \partial_\mu \omega^\mu$ term in the equations of motion, which should not change the time evolution of our fields, provided the gauge condition is always verified. This is in principle the case if the initial condition verifies the gauge condition. Numerically, the system tends to drift away from this condition and one needs to take additional precautions to enforce the gauge condition at all times.

To enhance stability, we introduce the ''electric'' and ''magnetic'' fields of ω, $\mathcal{E}_k = \partial_k \omega_0 - \dot{\omega}_k$, $\mathcal{M}_k = \epsilon_{klm} \partial_l \omega_m$, and eliminate ω_0 as a dynamical variable. The latter is possible because the mass enforces the gauge $\dot{\omega}_0 = \partial_k \omega_k$ leaving only three dynamical degrees of freedom for the ω field. This choice of variables allows us to use a local scheme, which gives the new time derivatives at a given spatial point as an implicit function of the local time derivatives and spatial derivatives only.

The Ψ equations of motion are in a form which ensures the chiral condition without having an explicit Lagrange multiplier. Numerically we use a leapfrog scheme which is discussed in further detail in the Appendix. We discretize the fields on a uniform spatial grid. The values of all fields at a given time step are defined on each grid point. The time derivatives of the fields are retarded with one half-time step. The time evolution of the fields themselves is thus straightforward. The velocities are evolved using the second-order equations of motion. This involves solving locally a set of coupled implicit equations, since the velocities also appear in the interaction terms.

In the Ψ scheme, our set of equations is

$$\begin{aligned}
\ddot{\Psi}^A &= \sum_k \partial_k^2 \Psi^A - \Psi^A \sum_E \left(\dot{\Psi}^{E^2} - \sum_k \partial_k \Psi^{E^2} \right) \\
&\quad + m_\pi^2 (\delta^{A0} - \Psi^A \Psi^0) + \frac{3g}{8\pi^2 f_\pi^2} \epsilon^{ABCD} \Psi^B \\
&\quad \times (\epsilon_{klm} \mathcal{E}_k \partial_l \Psi^C \partial_m \Psi^D + 2\mathcal{M}_k \dot{\Psi}^C \partial_k \Psi^D), \\
\dot{\mathcal{E}}_k &= -\epsilon_{klm} \partial_l \mathcal{M}_m - M^2 \omega_k \\
&\quad + \frac{3g}{8\pi^2} \epsilon_{klm} \epsilon^{ABCD} \Psi^A \dot{\Psi}^B \partial_l \Psi^C \partial_m \Psi^D, \\
\dot{\mathcal{M}}_k &= \epsilon_{klm} \partial_l \mathcal{E}_m, \\
\ddot{\omega}_k &= \dot{\mathcal{E}}_k + \partial_k \partial_l \omega_k. \qquad (17)
\end{aligned}$$

In addition, we compute ω_0 using the gauge condition and use it in the evaluation of the energy.

The technical setup of the calculations was the same as described in [9]. We used clusters of typically six to ten IBM SP-2 machines. For the final run we used a cluster of 20 machines. Our parallel codes are written in FORTRAN90. We use a variety of grid sizes. Our physical box is $10\times10\times10$ fm^3 for the calculation itself, but for the scaling analysis presented in Sec. III C it is significantly smaller, only $6\times5\times5$ fm^3. By taking advantage of the symmetry of the problem, we actually simulate only an eighth of the physical box. We used various grid sizes, from 8 to 20 points per fm, 12 points/fm for the main runs. We used time steps varying from 100 per fm to 3200 per fm in the violent regime. As initial conditions we use a static, spherically symmetric soliton whose profile we obtained in a separate calculation. We boost this configuration to $\beta = 0.5$ towards its mirror image created by the appropriate boundary conditions at the symmetry wall. The total initial energy of the two soliton system is then 1500 MeV, of which 1300 MeV is in the solitons and approximately 200 MeV is kinetic energy. Our initial velocity is slightly less than the one used in the previous study of annihilation [8] ($\beta = 0.63$) and the same used in our study of two-Skyrmion scattering, which was also in the range used in the Caltech study of scattering [13]. The choice of the initial separation is dictated by the need to minimize the overlap between the two solitons.

B. Results

Below we describe the process of the central annihilation of a Skyrmion and an anti-Skyrmion which are initially 3.0 fm apart and are boosted towards each other with an initial velocity of $\beta = 0.5$ each.

The process is best illustrated by the time evolution of the pion field. In Fig. 1 we plot the quantity $(1-\Psi_0)$ as a function of time. This choice is natural since in free space $\Psi_0 = 1$ and at the tip of a Skyrmion $\Psi_0 = -1$. In the first plot we have the essentially unmodified Skyrmion and anti-Skyrmion, slightly superimposed. The Ψ_0 component of the pion field is identical for the two objects. Charge conjugation and grooming affects only the ''spatial'' components.

In order to annihilate, the fields have to unwind;[2] therefore the field in the center point has to pass through the value $\Psi = (-1,0,0,0)$ (the highest point in our plots). In other words, the tips must merge before unwinding. The second frame illustrates a moment close to this situation. As will be discussed later, the axial dependence is rather sharp at this moment. In our simulation the symmetry center is between lattice points; therefore the crest in the second frame should be close to horizontal with a proper extrapolation.

From this point on, the value of Ψ_0 approaches fast the vacuum value as the topological obstacle is now gone. After another fm/c the field is close to the vacuum value (1,0,0,0). The variation is so fast that the field in the center ''overturns'' and increases again. Only after 3 fm/c from the passing of the peak do these large amplitude oscillations subside by propagating outwards as spherical waves. This outgoing pion radiation is clearly seen in the final two frames of Figures 1, 5, and 6.

[2]Because of symmetry, on the central axis the field is always of the form $\Psi = (\cos\theta, \sin\theta, 0, 0)$. As one passes through the center of a Skyrmion, the angle rotates through a full circle. For the anti-Skyrmion, the winding is opposite. As the two objects approach, the center point unwinds.

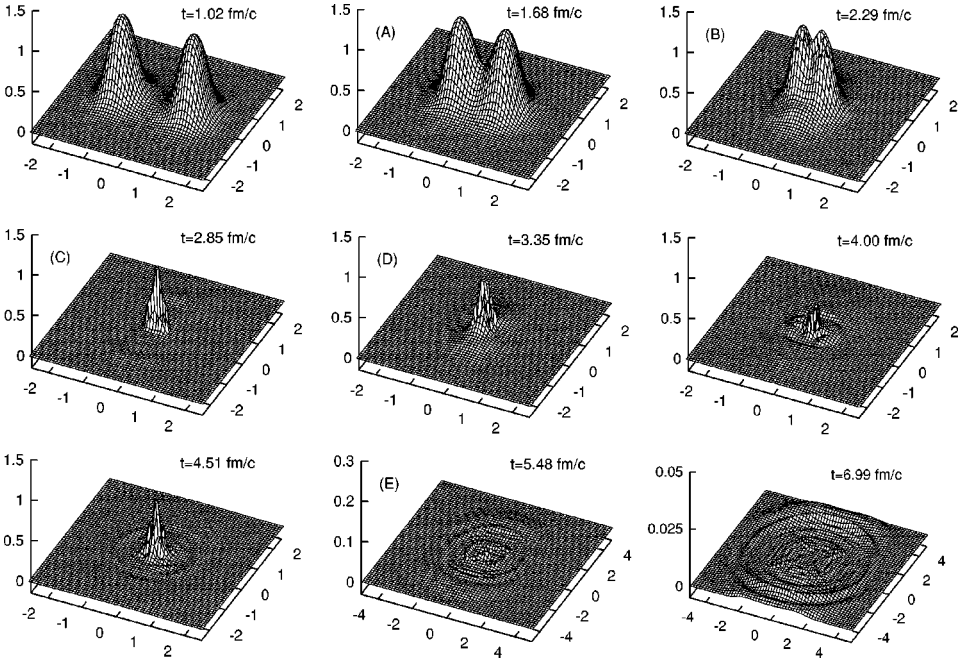

FIG. 1. One component of the pion field $(1-\Psi_0)$ at various moments during annihilation. The fields are shown in the xy plane. The x axis is the direction closer to horizontal. The length on the axes is measured in fm. The quantity we plot is dimensionless. Note the different vertical and horizontal scales in the last two frames.

The time evolution of the baryon number is illustrated in Fig. 2. We compute the baryon number by integrating Eq. (5) in one half-space. The baryon number in the other half-space is equal and opposite to this. The annihilation starts basically when the Skyrmions touch, at $t=1.66$ fm (point A in Fig. 2). In the absence of interactions, exactly half of the baryon number in one half-space should annihilate when the two centers coincide, at $t=3.0$ fm/c . Because of the attractive interaction, this happens a little faster, at around $t=2.3$ fm/c (B). Along with the field, the remaining baryon number decreases quickly to zero ($t=2.85$ fm/c, point C), continues to decrease for a short time, and then oscillates, hitting an absolute minimum at point (D). The baryon number oscillates along with the large amplitude oscillations of the field and finally settles at zero ($t=5.5$ fm/c, point E) in the radiation regime.

Altogether, the unwinding of the field (from A to C) takes approximately 1.2–1.3 fm/c, but this is followed by localized oscillations which take a longer amount of time (from C to E, approximately 2.5 fm/c), therefore the total process from the moment when the Skyrmions touch to the complete disappearance of the baryon number takes about 3.5 fm/c, depending on the choice of the point E.

In Fig. 3 we plot the baryon density and the x component of the baryon current, integrated in the yz plane, as a function of the x coordinate. This also illustrates the progress of the annihilation. The two charge concentrations practically disappear at C. We can see that the current increases in the center, starting from half-annihilation B, peaks shortly after total annihilation C, and then oscillates.

In Fig. 4 we plot the evolution of the energy as the sum of the energy in the pion field and the omega field. The dotted lines and labels A–E in Fig. 4 indicate the same times as in Fig. 2. Our definitions of the energy densities—which are integrated numerically to give the quantities in Fig. 4—are

$$\mathcal{H}_\pi=\frac{1}{2}\left(\dot{\Psi}^A\dot{\Psi}^A+\sum_{k=1}^{3}\partial_k\Psi^A\partial_k\Psi^A\right),$$

$$\mathcal{H}_\omega=\frac{1}{2}\sum_{k=1}^{3}(M_\omega^2\omega_k^2+\mathcal{M}_k^2+\mathcal{E}_k^2)+\frac{1}{2}M_\omega^2\omega_0^2. \tag{18}$$

The piece corresponding to the ω_0 field can be defined in terms of our dynamical variables

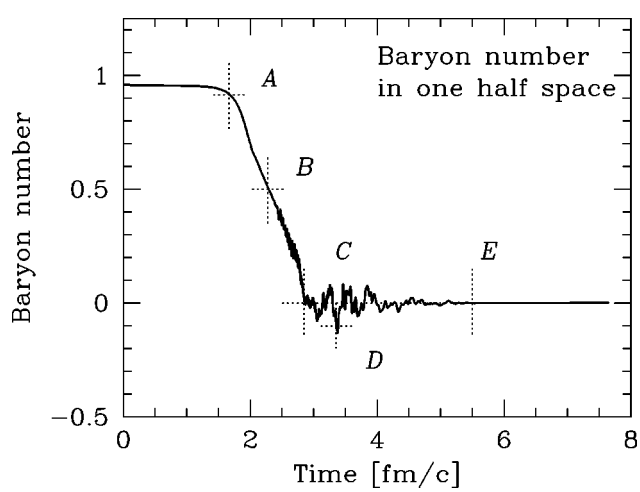

FIG. 2. Evolution of the baryon number in one half-space during a central annihilation process. The points A–E indicate particular moments which are also indicated in Figs. 1, 4, and so on, and are referred to throughout the text. Note especially point B, which corresponds to ''half-annihilation.'' It is associated with the merging of two topological centers and also marks the beginning of the violent part of the annihilation process.

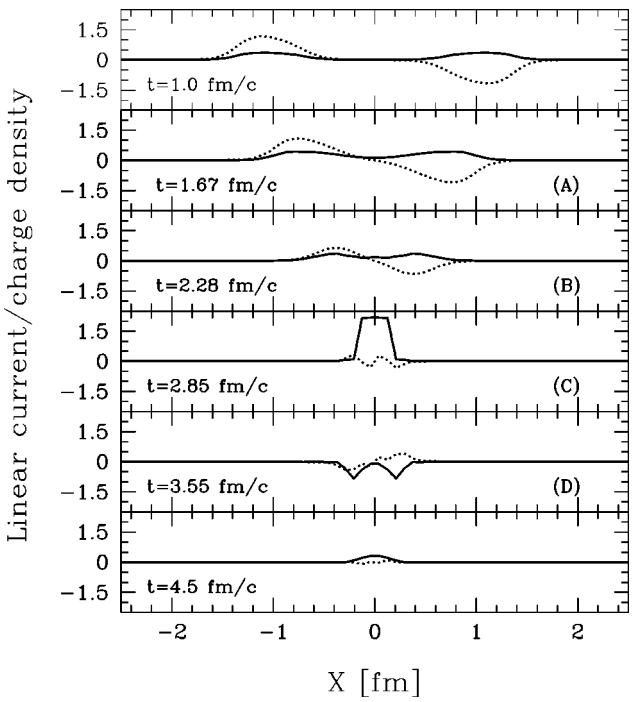

FIG. 3. The baryon number density (dotted lines) and the x component of the baryon current density (solid lines), integrated over y and z (in fm^{-1} and c/fm, respectively), as a function of the x coordinate, at various moments during the annihilation process.

$$\mathcal{H}_{\omega_0}=\frac{1}{2}M_\omega^2\omega_0^2=\frac{1}{2M_\omega^2}\left[\left(\frac{3g}{2}B_0\right)-(\partial_k\mathcal{E}_k)\right]^2. \qquad (19)$$

The second identity follows from the equations of motion for ω_0, the definition of $\mathcal{E}_k$, and the gauge condition.[3] We also plot the total energy in Fig. 4. There is a loss of less than 100 MeV from a total of 1500 MeV between the points B and E, which corresponds to approximately 7%.[4] We assign this loss to numerical dissipation which is significant in the fast-varying regime between half-annihilation (B) and the onset of the radiation regime (E). The further decay of the total energy simply corresponds to outgoing radiation which leaves the simulation box.

The annihilation process is accompanied by the rearrangement of the energy between the pion and omega sectors. Initially we have free-space propagation of the solitons. The smooth part of the unwinding beginning at (A) is accompanied by the flow of energy from the pion field into the omega sector. The net flow stops before full unwinding (C) and

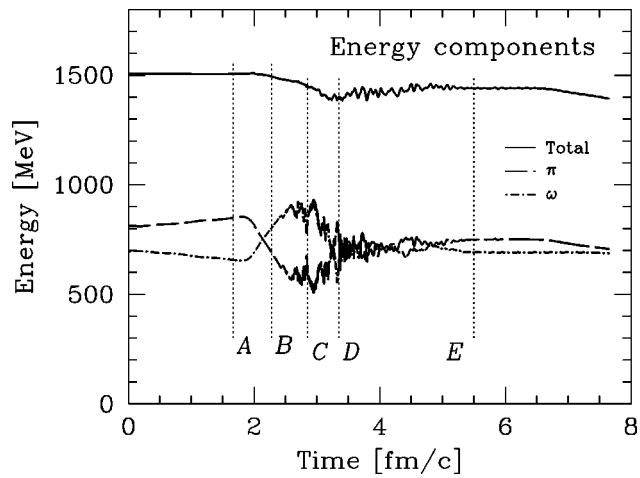

FIG. 4. Evolution of the energy and its components during a central annihilation process.

yields to oscillations which correspond in time to the large oscillations of the field, accompanied by significant oscillations of the baryon number around zero. During this regime, when the net baryon number oscillates, the energy also flows back and forth between the two sectors. Eventually the two sectors stabilize after E at comparable values.

A more detailed picture of the energy flow is given by looking at the spatial distribution of the energy at various moments. In Fig. 5 we plot the total energy density. In the first three frames we see the two configurations approaching each other, then merging. Starting from the third frame, which roughly corresponds to half-annihilation, the energy density in the center becomes very large, almost δ-function-like. Eventually the energy starts to flow outwards in concentric waves. In the latter frames, even though there is still a spike in the center, most of the energy is in the outgoing waves. This is seen better in Fig. 6 where we plot the total energy density multiplied by the distance ρ to the symmetry axis for the last three frames of Fig. 5. Plotting $\rho\times dE/dV$ gives a better estimate of the relative amount of energy contained in different regions of space.

The energy density plots reveal two important aspects. First is the fact that the energy density is extremely high in the center between $t=2.3$ fm/c and $t=5.0$ fm/c, which is the period between annihilation and the start of significant outward radiation. The other important feature is the abundance of fast, small-amplitude oscillations which persist to the end of the time interval under consideration. These oscillations originate in the period immediately following annihilation when there is a very fast, global variation of the fields confined to a small region of space. Most likely, numerical error stemming from the large local variations has the role of a source for these oscillations. However, as discussed in the next subsection on numerical stability, the persistence of the small oscillations is also possibly due to properties of the exact, continuum equations of motion.

Despite the presence of the small oscillations, there is a well-defined pattern to the flow of energy, both in terms of the radial flow and angular distribution. Starting with $t=2.5$ fm/c, the energy is concentrated in a small region (ini-

[3]Numerically this identity is violated because the right-hand side is the difference of two large numbers in the fast-varying regime. The identity relies on third-order derivatives of our dynamical quantities. However, using ω_0 computed from the gauge condition leads to reasonable energy conservation.

[4]The loss in the run presented in this section is less, actually closer to 5%, but the runs presented in the next section, which use a smaller physical box and slightly different initial conditions, lose about 100 MeV.

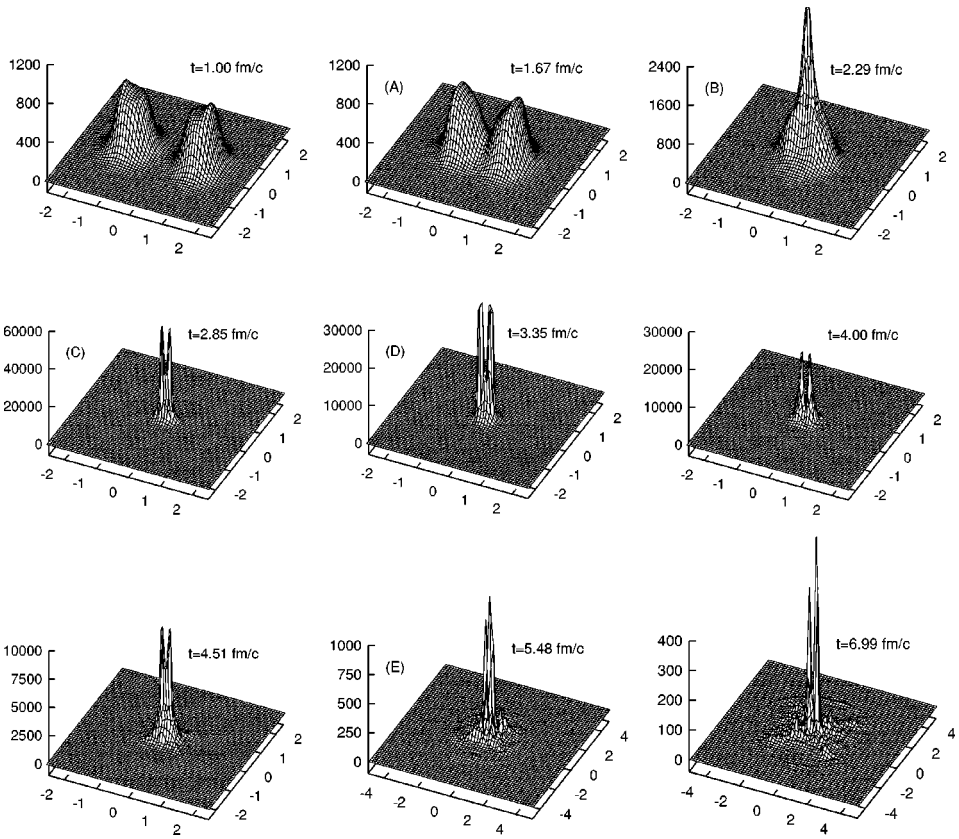

FIG. 5. The total energy density at various moments during annihilation, in MeV/fm^3. The density is shown in the xy plane. The x axis is the direction closer to horizontal. The length on the axes is measured in fm. Note the different vertical and horizontal scales in the various frames.

tially of radius 1 fm) around the center. The distribution becomes very strongly peaked in the time between half-annihilation and complete unwinding. There is some outgoing radiation as early as $t=3.5$ fm/c but the strongly peaked pattern eases up only after $t=5.0$ fm/c when the bulk of the energy starts flowing outward.

The macroscopic flow of energy is nicely illustrated in Fig. 7 by plotting the total energy contained in spherical shells surrounding the center. Initially we have the two incoming solitons which move through bins in decreasing order of radius. Starting from $t=2.5$ fm/c the energy accumulates in the center bin (a sphere of radius 0.5 fm/c, half the linear size of a Skyrmion). The accumulation peaks at about $t=3$ fm/c when this bin contains more than 2/3 of the total energy. Even though the outward flow starts as early as $t=3.0$ fm/c, it becomes significant only later. Approximately 90% of the energy leaves the center sphere by $t=6.0$ fm/c, or 3.0 fm after full unwinding. From then on, we can follow the energy moving outwards through bins of increasing radius. We can also understand how the decrease in total energy (top panel, same line as in Fig. 4) is really just flow leaving the simulation box.

Finally, in Fig. 8 we illustrate the angular distribution of the energy during the annihilation process. We can see a depletion of the small angle bins and a peak around 45° which seems to be the preferred direction of the energy flow. It should be noted that these angular distributions are in a plane, but that the three-dimensional distribution has cylindrical symmetry about the direction of collision. The axial symmetry precludes the formation of a torus intermediate state as seen in Skyrmion-Skyrmion scattering, and in fact we see no evidence in our calculation of such an intermediate state. The suppression of small angle bins is reminiscent of the pattern seen in baby Skyrmion annihilation [14], while an enhancement at 45° has not been previously noted to our knowledge. Given the fact that the dynamics of soliton scattering in two [15] versus three dimensions [13,9] both allow for scattering at 90° but through qualitatively different inter-

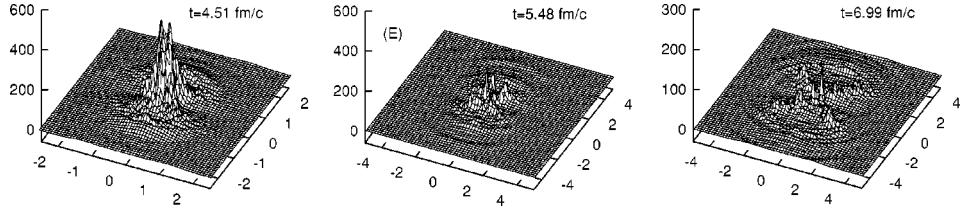

FIG. 6. The total energy density multiplied by the distance to the symmetry axis, in MeV/ fm^2, at various moments during the latter part of annihilation. The density is shown in the xy plane. The x axis is the direction closer to horizontal. The length on the axes is measured in fm.

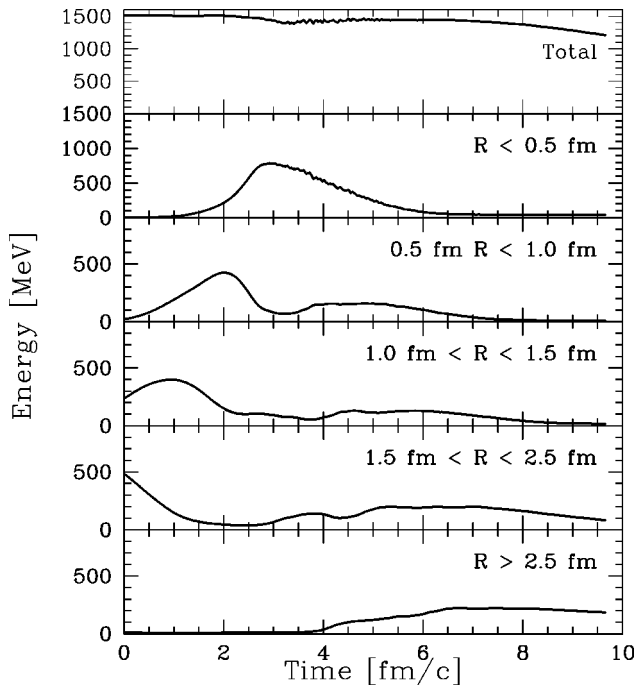

FIG. 7. Total energy in spherical shells surrounding the annihilation as a function of time.

mediate states, neither the suppression of the small angles nor the peak around 45° is surprising.

C. Checks

In this subsection we investigate the extent to which our results are influenced by the details of the numerical calculation. This aspect is particularly important because of the presence of large time and spatial derivatives of the fields. The macroscopic dynamics of the problem imposes a certain minimum size for the simulation box (a cube of size 5 fm). We use a fixed grid. This limits the number of points per fm we can have to not much more than 20. Our typical calculations use 12 points per fm.

One obvious concern stems from the fact that we were able to ensure energy conservation only to about 7%, at best 5%. Approximately 70–100 MeV of the total initial energy of 1500 MeV is lost to numerical dissipation, as can be seen in Figs. 4 and 7. This loss comes between points B and C in the respective plots, and is a significant but not alarming energy loss.

Numerical error is probably also responsible for the appearance of persistent but random oscillations. Starting with $t=4.0$ fm/c, the field configurations display oscillations on the scale of a few lattice spacings. This is preceded by a configuration which is probably singular in the continuum limit, at half-annihilation (we discuss this in a separate section). This raises the question of whether the continuum physics we wish to study mixes with lattice artifacts or, rather, whether we are able to extract continuum physics reliably.

To test the stability of our results, we performed several runs using the π algorithm for a number of different lattice spacings. The results obtained with this algorithm with identical box size and initial conditions are very similar to those obtained with the Ψ algorithm. The program based on the π algorithm has been readily available for a longer time, and we used it for the very time consuming runs with larger numbers of points. Below we present results for 12, 16, and 20 points per fm. The physical process in these runs is the same, i.e., head-on annihilation with the same parameters as in the main run, initial separation of 3 fm, initial velocity of $\beta=0.5$. However, we used the smallest possible simulation box, only $6\times5\times5$ fm^3, and a slightly different initial configuration. Using an even smaller box would have resulted in more energy dissipation outside the box and, most notably, reflection off the walls (which we are unable to eliminate completely) which would interfere with the ''real'' physics. We then compared the results from these various runs. Ideally, the numerical artifacts should scale away as the lattice spacing is decreased.

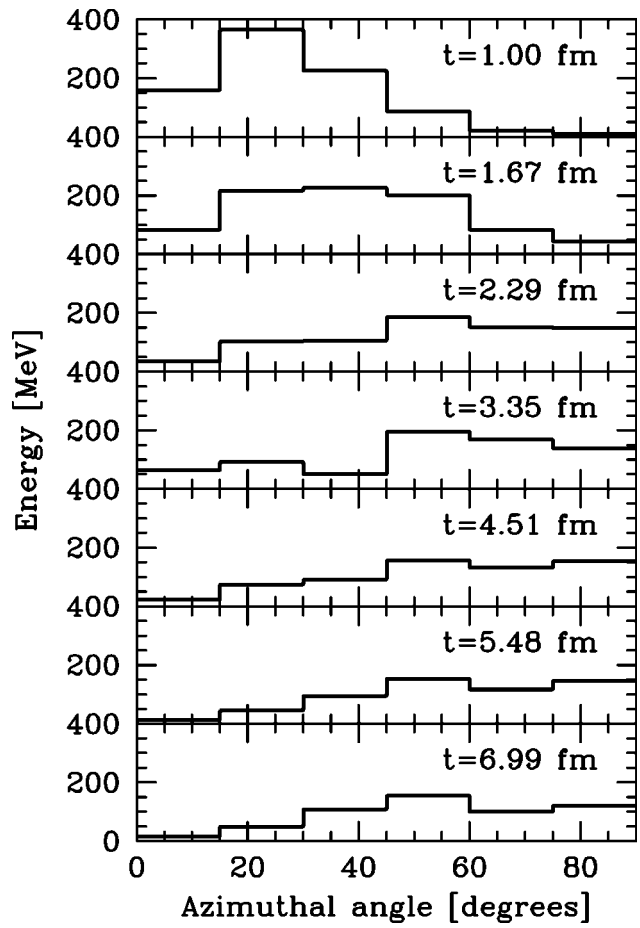

FIG. 8. Total energy in angular intervals measured from the symmetry axis at various moments during annihilation.

In Fig. 9 we plot the total energy for three runs which are identical (including the time step, which is decreased before $t=3.0$ fm/c from 100 per fm to 3200 per fm/c) except for the lattice spacing which is, respectively, $N=12,16,20$ points per fm. We zoomed in on the interval between $t=2.0$ fm/c and $t=5.0$ fm/c, when most of the dissipation takes place. The energy decreases as the system is squeezed into the

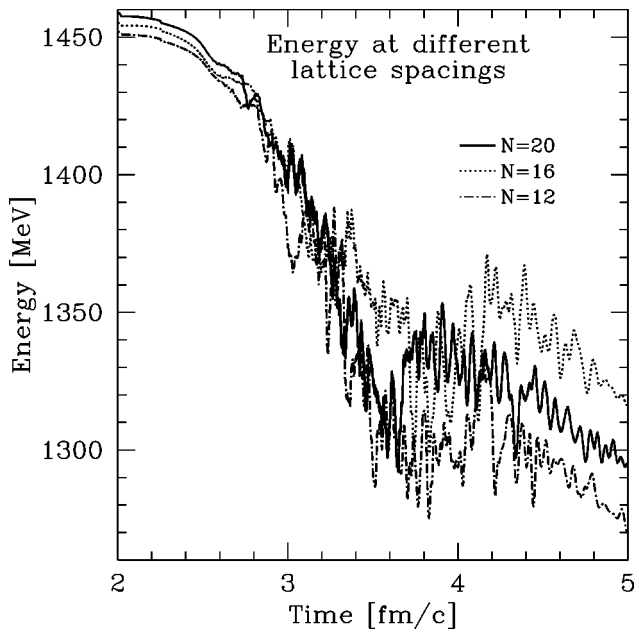

FIG. 9. The total energy during the more violent part of the annihilation process, in three calculations which are identical except for the number of points per fm, N. Note that these runs are slightly different from the runs discussed in the preceding section. They are performed in a smaller box using a slightly different initial configuration.

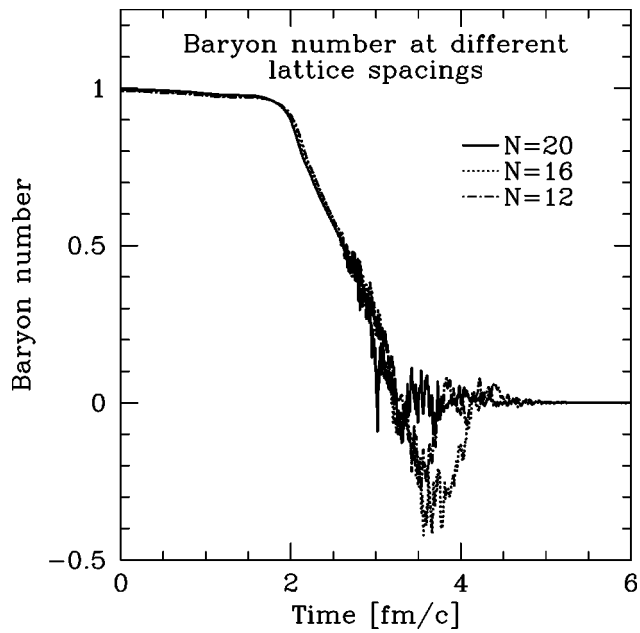

FIG. 10. The baryon number in one half-space during the annihilation process, in three calculations which are identical except for the number of points per fm, N.

small region around the center. The loss is likely caused by discretization error. However, as the system expands, only a fraction of the loss is recovered. The same run with $N=8$ points per fm, which we cannot plot on the same graph without making the graph completely unintelligible, gives worse conservation than all three runs plotted here. The two larger spacings do give better energy conservation then the $N=12$ run, as one would expect. However, there is no clear scaling, as the order of the $N=16$ and $N=20$ results is reversed. As an argument for the reliability of our calculations, let us emphasize that we are talking about differences of 30 MeV here between calculations, i.e., 2% of the total energy.

A look at the comparative plot of the baryon number in the same runs reveals a similar picture (Fig. 10). In all three runs shown, the remarkable points A,B, C, and E, i.e., the start of the unwinding, the point of half-annihilation, and full unwinding, as well as the end of the violent fluctuations, practically coincide. However, the extent and duration of the excursion of the baryon number below zero varies. It is practically absent for $N=8$ but there is a large fluctuation later on (again, not plotted). For $N=12$ and $N=16$ we see a sizable excursion, larger for $N=16$, but again the $N=20$ calculation is out of sequence and has only a small negative excursion. It could be that the time step choice (same for all runs) is too large for $N=20$. Even with this in mind, the overall evolution of the baryon number is very similar for the four runs we discussed. The decay of the baryon number and the duration of the large oscillations is a robust feature of the calculation. Furthermore, the small oscillations seem to be very noisy with little relationship from grid size to grid size.

The outward energy flow is perhaps the most important quantitative result one may extract from a numerical calculation of Skyrmion–anti-Skyrmion annihilation. This result would be the starting point for constructing the final pion and omega states in a calculation of low-energy $N\bar{N}$ annihilation [5]. In Fig. 11 we plot the energy contained in centered spherical shells, for the three $N=12,16,20$ calculations dis-

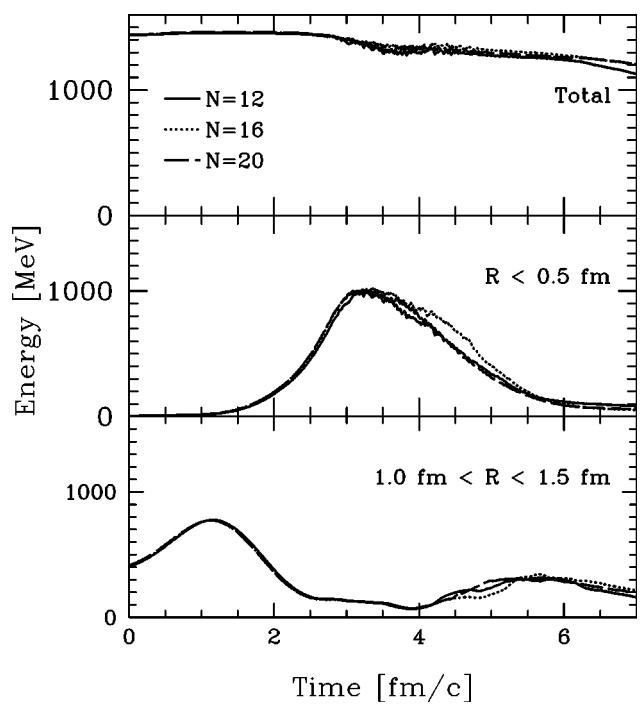

FIG. 11. Evolution of the energy contained in a few spherical shells for various lattice spacings.

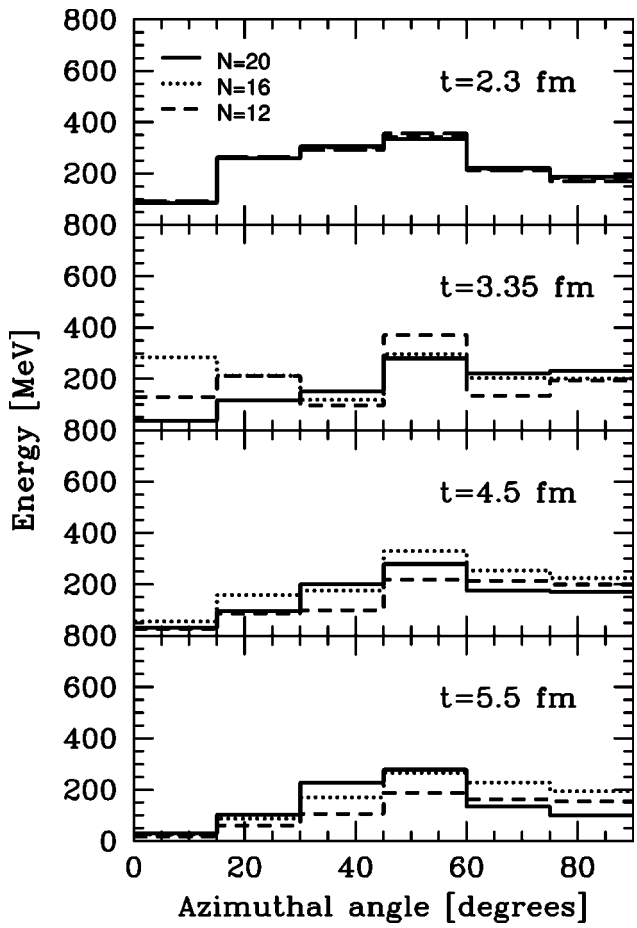

FIG. 12. Evolution of the energy contained in angular bins for various lattice spacings.

cussed above. The evolution of the energy contained in the shells is practically the same for the three runs. There is some fluctuation, especially for the center bin, but the differences are not very large. In particular there is little difference in the bins at larger distance, and that is where information would be extracted for the outgoing pion and omega states.

In Fig. 12 we plot the energy contained in angular bins measured from the x axis. These plots show more variation with the lattice spacing then the radial bins shown in Fig. 11 but this is partially due to the way the energy in a given angular bin is determined.[5] Still, the significant differences seen at $t=3.35$ fm/c subside by the time the radiation regime starts. The suppression at small angles and the maximum around 45° are present in all three runs.

In conclusion, while our detailed results are somewhat sensitive to the number of lattice points, the physically important observables, energy conservation, the time evolution of the baryon number, and the flow of energy are reasonably well determined and do not depend strongly on variations in the number of lattice points. In future studies of annihilation we will use a separate grid in the spatial region where the violent behavior is concentrated, which should allow for significantly smaller lattice spacings.

[5]This is done here by extrapolating the energy density from the xy plane of points closest to the symmetry center, assuming cylindrical symmetry.

IV. STABILITY ANALYSIS

One of the two most prominent features of our results is the appearance of persistent, small-amplitude oscillations after unwinding. These oscillations are present practically to the end of our calculations. In the early post-unwinding regime they influence the total energy and baryon number.

The frequency of the fluctuations of the total energy and baryon number increases with the number of lattice points, suggesting that these are numerical artifacts. We have been forced to use extremely small time steps in our runs (thousands of time steps per fm). However, the precautions we took did not eliminate these oscillations. On the other hand, we are able to perform our simulations to a robust end even in the presence of these oscillations. Furthermore, the macroscopic (long-wavelength) aspects of the outputs are not strongly influenced by the number of points, suggesting that numerical artifacts do not overwhelm the continuum physics.

The lack of success of earlier attempts to simulate annihilation [7,8,6] has been blamed on a situation which arises in the Skyrme model [7]. Because of the nonlinear nature of the interaction term, the equations of motion may cease to be of hyperbolic nature, i.e., have second time and spatial derivative terms of opposite signs. Hyperbolic equations of motion ensure the existence of plane-wave-like solutions (of the form $e^{ik_\mu x^\mu}$ with real wave number $k=\sqrt{\vec{k}\cdot\vec{k}}$) which may propagate as packets of quasiconstant amplitude. If the sign of the second time derivative reverses, the wave number may become imaginary for a given wave vector $\vec{k}$, resulting in waves with exponentially increasing amplitude. A small fluctuation that excites this mode would then result in a large change in the final result. In other words, if the equations of motion are not hyperbolic, the system in unstable. For a detailed derivation of the instability for the Skyrme model of just this sort, we refer to [7].

In the following we investigate the possibility of such an instability occurring in our model. Recall that we are using ω stabilization rather than a Skyrme term in order to avoid the damage brought on by the fourth-order interaction term. Consider our equations of motion

$$\begin{aligned}\partial_\mu\partial^\mu\Psi^A-\Psi^A(\Psi^E\partial_\mu\partial^\mu\Psi^E)&\\ =\frac{3g}{8f_\pi^2\pi^2}\epsilon^{\mu\nu\alpha\beta}\epsilon^{ABCD}\partial_\nu\omega_\mu\Psi^B\partial_\alpha\Psi^C\partial_\beta\Psi^D&\\ +m_\pi^2(\delta^{A0}-\Psi^0\Psi^A),&\\ \partial^\nu\partial_\nu\omega^\mu=\frac{g}{8\pi^2}\epsilon^{\mu\nu\alpha\beta}\epsilon^{ABCD}\partial_\nu\Psi^A\Psi^B\partial_\alpha\Psi^C\partial_\beta\Psi^D&\\ -M^2\omega^\mu.&\end{aligned}\tag{20}$$

Consider now a solution of these equations and a small, fast-varying perturbation added to it:

$$\Psi^A \to \Psi_0^A + \epsilon\phi^A, \quad |\partial_\mu \phi^A| \gg |\partial_\mu \Psi^A|,$$
$$\omega^\mu \to \omega_0 + \epsilon\sigma^\mu, \quad |\partial_\mu \sigma_\nu| \gg |\partial_\mu \omega_\nu|, \tag{21}$$

where ϵ is a small real number. We study the stability of the equations of motion by analyzing the behavior of these small perturbations in the background field given by $\{\Psi^A, \omega^\nu\}$. First, we substitute the ansatz (21) into the equations of motion and expand to first order in ϵ:

$$\begin{aligned}\partial_\mu\partial^\mu\phi^A &+ \phi^A(\partial_\mu\Psi^E\partial^\mu\Psi^E) + 2\Psi^A(\partial_\mu\phi^E\partial^\mu\Psi^E)\\ &= \frac{3g}{8\pi^2 f_\pi^2}\epsilon^{\mu\nu\alpha\beta}\epsilon^{ABCD}\{\partial_\nu\sigma_\mu\Psi^B\partial_\alpha\Psi^C\partial_\beta\Psi^D\\ &\quad + \partial_\nu\omega_\mu(\phi^B\partial_\alpha\Psi^C\partial_\beta\Psi^D + 2\Psi^B\partial_\alpha\phi^C\partial_\beta\Psi^D)\}\\ &\quad - 2m_\pi^2(\phi^A\Psi^0 + \Psi^A\phi^0),\end{aligned}$$

$$\partial_\nu\partial^\nu\sigma^\mu = \frac{3g}{8\pi^2}\epsilon^{\mu\nu\alpha\beta}\epsilon^{ABCD} \times\left(\partial_\nu\phi^A\Psi^B + \frac{1}{3}\partial^\nu\Psi^A\phi^B\right)\partial_\alpha\Psi^C\partial_\beta\Psi^D. \tag{22}$$

We must again remember that the variation of Ψ is constrained:

$$(\Psi^A + \epsilon\phi^A)(\Psi_A + \epsilon\phi_A) = 1 + \mathcal{O}(\epsilon^2) \to \phi^A\Psi^A = 0. \tag{23}$$

Therefore the quantity $\epsilon^{ABCD}\partial_\nu\Psi^A\phi^B\partial_\alpha\Psi^C\partial_\beta\Psi^D$ has to vanish since it is the quadruple product of four isospin vectors which are all perpendicular on $\mathbf{\Psi}$.

We now assume that small perturbations are well approximated by plane waves,

$$\phi^A = \Phi^A e^{ik_\mu x^\mu}, \quad \sigma^\nu = \Sigma^\nu e^{ik_\mu x^\mu}, \tag{24}$$

and attempt to obtain equations for the wave vector k_μ. If the equations have solutions which correspond to an imaginary $k_0 = \Omega$, then we conclude that our equations of motion are unstable, since they allow for the exponential increase of a small perturbation. After substituting the ansatz (24) into Eq. (22) and contracting the first equation with Φ^A we obtain

$$\begin{aligned}&-k_\mu k^\mu + M_\perp^2 + 2m_\pi^2\Psi^0\\ &\quad = \frac{3g}{8\pi^2 f_\pi^2} ik_\nu\Sigma_\mu\epsilon^{\mu\nu\alpha\beta}\epsilon^{ABCD}\Phi^A\Psi^B\partial_\alpha\Psi^C\partial_\beta\Psi^D,\\ &(-k_\nu k^\nu + M^2)\Sigma^\mu\\ &\quad = \frac{3g}{8\pi^2} ik_\nu\epsilon^{\mu\nu\alpha\beta}\epsilon^{ABCD}\Phi^A\Psi^B\partial_\alpha\Psi^C\partial_\beta\Psi^D.\end{aligned} \tag{25}$$

Here we took advantage repeatedly of the perpendicularity of $\mathbf{\Phi}$ to $\mathbf{\Psi}$. We also defined $M_\perp^2 = \partial_\mu\Psi^E\partial^\mu\Psi^E$. Note that this quantity originates in the constraint on $\mathbf{\Psi}$ and is not necessarily positive definite. This in itself does *not* imply the appearance of an instability, since in the static case, which is free of instabilities against small oscillations, $M_\perp < 0$. We should of course take the sign of $M_\perp$ into account when we analyze the characteristic equation.

Let us solve the second equation for the polarization vector Σ^μ and substitute into the first equation. The result can be rearranged as follows:

$$\begin{aligned}&(-k_\mu k^\mu + M^2)(-k_\rho k^\rho + M_\perp^2 + 2m_\pi^2\Psi^0)\\ &\quad = -\left(\frac{3g}{8\pi^2 f_\pi}\right)^2 k_\nu k_\rho\epsilon^{\mu\nu\alpha\beta}\epsilon_\nu^{\rho\sigma\tau}V_{\alpha\beta}V^{\sigma\tau}\\ &\quad = -\left(\frac{3g}{8\pi^2 f_\pi}\right)^2 k_\nu k_\rho S^{\mu\nu}S_\mu^\rho,\end{aligned} \tag{26}$$

where we have defined $V_{\alpha\beta} = \epsilon^{ABCD}\Phi^A\Psi^B\partial_\alpha\Psi^C\partial_\beta\Psi^D$ and $S^{\mu\nu} = \epsilon^{\mu\nu\alpha\beta}V_{\alpha\beta}$.

As for any Lorentz tensor of rank 2, there are two invariants one may construct from the components of $S^{\mu\nu}$: $A = \epsilon^{\mu\nu\alpha\beta}S_{\mu\nu}S_{\alpha\beta}$ and $B = S^{\mu\nu}S_{\mu\nu}$. If $A = 0$, then using the appropriate Lorentz boost, the tensor can be either brought to a form where the ''electric'' components S^{0k} vanish or it can be brought to a form where the ''magnetic'' components S^{lm} vanish. Only one of these situations is possible, depending on the sign of the other invariant. If $B < 0$, the tensor is ''electric,'' and if $B > 0$, it is ''magnetic.'' Let us compute the first invariant:

$$\begin{aligned}A &= \epsilon^{\mu\nu\alpha\beta}\epsilon_{\alpha\beta\rho\sigma}\epsilon_{\mu\nu\lambda\tau}V^{\rho\sigma}V^{\lambda\tau}\\ &= 2\epsilon_{\mu\nu\lambda\tau}V^{\mu\nu}V^{\lambda\tau}\\ &= 2\epsilon^{ABCD}\epsilon^{EFGH}\Phi^A\Psi^B\Phi^E\Psi^F\epsilon^{\mu\nu\alpha\beta}\\ &\quad \times\partial_\mu\Psi^C\partial_\nu\Psi^D\partial_\alpha\Psi^G\partial_\beta\Psi^H.\end{aligned} \tag{27}$$

Consider one set of values for the eight isospin indices on the right-hand side. For a nonvanishing term, the labels $\{C,D,G,H\}$ must be all different: otherwise we would have symmetry in two Greek indices. For simplicity let $\{C,D,G,H\} = \{0,1,2,3\}$. The Lorentz sum remaining to be performed can be rearranged:

$$\begin{aligned}&\epsilon_{0123}\epsilon^{\mu\nu\alpha\beta}\partial_\mu\Psi^0\partial_\nu\Psi^1\partial_\alpha\Psi^2\partial_\beta\Psi^3\\ &\quad = \epsilon_{ABCD}\epsilon^{0123}\partial_0\Psi^A\partial_1\Psi^B\partial_2\Psi^C\partial_3\Psi^D\\ &\quad = 0.\end{aligned} \tag{28}$$

The term on the right-hand side vanishes because it contains four isovectors perpendicular to Ψ. Hence the first invariant vanishes. The second invariant is

$$\begin{aligned}B &= S^{\mu\nu}S_{\mu\nu}\\ &= \epsilon^{\mu\nu\alpha\beta}\epsilon_{\mu\nu\rho\sigma}V_{\alpha\beta}V^{\rho\sigma}\\ &= -2V_{\alpha\beta}V^{\alpha\beta}\\ &= 2[V_{0k}V_{0k} - V_{lm}V_{lm}]\end{aligned}$$

$$= 2\epsilon^{ABCD}\epsilon^{EFGH}\Phi^A\Psi^B\Phi^E\Psi^F[2\dot{\Phi}^C\partial_k\Psi^D\dot{\Phi}^G\partial_k\Psi^H - \partial_l\Psi^C\partial_k\Psi^D\partial_l\Psi^C\partial_k\Psi^D]. \tag{29}$$

In the last line we have lowered all Lorentz indices. [We remind the reader of our convention $A_\mu=(A_0,\vec{A})$, $A^\mu=(A_0,-\vec{A})$.] It is clear that if the time derivatives are small, $B<0$, and if they are large, i.e., for fast-varying Ψ fields, $B>0$.

Let us consider the case with small time derivatives. Then, $B<0$ and the tensor S may be boosted so that $S_{lm}=0$. The characteristic equation is then

$$(M^2-k_\mu k^\mu)(M_\perp^2+2m_\pi^2\Psi^0-k_\nu k^\nu) = -2\mathcal{C}^2\{k_0k_0S^{l0}S_l^0+k_lk_mS^{0l}S^{0m}\},$$

$$(M^2+p^2-\omega^2)(M_\perp^2+2m_\pi^2\Psi^0+p^2-\omega^2) = 2\mathcal{C}^2\left\{\omega^2\sum_l (S_{0l}^2)-p_lp_m(S_{0l}S_{0m})\right\}. \tag{30}$$

Only the component of $\vec{p}$ parallel to the electric field vector $\{E_k=S_{0k}\}$ contributes to the right-hand side. Denoting that component by p_1, we have finally

$$(M^2+p^2-\omega^2)(M_\perp^2+2m_\pi^2\Psi^0+p^2-\omega^2) = 2\mathcal{C}^2(S_{0k}S_{0k})(\omega^2-p_1^2). \tag{31}$$

When the time derivatives dominate, we have $B>0$ and we may choose a reference frame where $S_{0k}=0$. The corresponding characteristic equation is

$$(M^2-k_\mu k^\mu)(M_\perp^2+2m_\pi^2\Psi^0-k_\nu k^\nu) = -2\mathcal{C}^2k_lk_mS^{jl}S_j^m = 2\mathcal{C}^2p_lp_mS_{jl}S_{jm}=2\mathcal{C}^2\sum_j\left(\sum_l p_lS_{jl}\right)^2 \geqslant 0. \tag{32}$$

The matrix $\mathcal{W}_{lm}=S_{jl}S_{jm}$ can be diagonalized $\tilde{\mathcal{W}}_{lm}=\delta_{lm}w_l$ and its eigenvalues will be real and positive as is obvious from the preceding equation. In that basis, the characteristic equation is

$$(M^2+p^2-\omega^2)(M_\perp^2+2m_\pi^2\Psi^0+p^2-\omega^2)=2\mathcal{C}^2\sum_l p_l^2w_l. \tag{33}$$

The characteristic equations in the $B<0$ and $B>0$ cases can be summarized as follows:

$$(M_1^2+p^2-\omega^2)(M_2^2+p^2-\omega^2)=K_1^2(\omega^2-P_1^2)\ [B<0],$$

$$(M_1^2+p^2-\omega^2)(M_2^2+p^2-\omega^2)=K_2^2P_1^2\ [B>0]. \tag{34}$$

Here, p^2 and P_1^2 are, respectively, the square and the square of one component of the arbitrary wave vector $\vec{p}=\vec{k}$ associated with the plane-wave perturbation. The quantities K_1^2 and K_2^2 are positive real numbers, and so is $M_1^2=M_\omega^2$. The only exception is $M_2^2=M_\perp^2+2m_\pi^2\Psi^0\approx M_\perp^2=\partial_\mu\Psi^E\partial^\mu\Psi^E$. As we have mentioned, $M_\perp^2$ is negative for a static field configuration such as a Skyrmion at rest, which does not exhibit a proliferation of small-wavelength perturbations. $M_\perp^2$ becomes positive when the time derivatives become large. This is the case in the center between the moments (B) and (E) (as defined in Sec. III), when most of the violent behavior takes place. It is clear from the sign of $M_\perp^2$, as well as from the following discussion, that the characteristic equations allow for a complex ω in a number of dynamical situations. We will focus on the regime between the moments (B) and (E) and assume $M_\perp^2>0$, and look for the conditions that are consistent with a negative ω^2.

In both cases ($B>0$ or $B<0$) we have a quadratic equation for ω^2. We may solve the characteristic equation for the time constant $\omega=k_0$ using any given $\vec{p}$. We remind the reader that we are studying the possibility of having a complex time constant. Such a perturbation would grow or decrease exponentially with time. When the right-hand side (RHS) is small, both solutions $\omega^2=M_1^2,M_2^2$ are real and positive, leading to stable oscillations.

In the $B<0$ case, the RHS has the effect of increasing both the coefficient of ω^2 (in absolute value) and the free term. Considering the solutions of a quadratic equation $aX^2-bX+c=0$ (all coefficients are positive here), $X_{12}=[(-b\pm\sqrt{b^2-4ac}]/2a$, it is clear that increasing b (if both a and c are positive) can make the positive real roots neither negative nor complex. Increasing c actually has the effect of bringing the roots closer together, therefore increasing the lower one. This may lead to trouble if the coefficient $c\geqslant b^2/4a$; however, this is not possible as is obvious if one writes the discriminant out explicitly. We conclude that in this case both solutions for ω^2 are real and positive, leading only to stable modes.

In the $B>0$ case there is no term containing ω on the right-hand side. However, the free term has the opposite sign compared to the previous case. It may not make the discriminant negative since it decreases c. However, if large enough in magnitude, this term may change the sign of c, thus allowing for a negative solution for ω^2 .

We conclude that if $M_\perp^2>0$, modes with purely imaginary ω^2 may occur in the $B>0$ case. This makes sense, because this case is associated with large time derivatives, exactly what characterizes our violent regime. The latter is also consistent with the assumption $M_\perp^2>0$. The sign of B is not immediately obvious, since it also depends on the polarization vector of the supposed perturbation, Φ^A: $B=\Phi^A\Phi^B\mathcal{T}^{AB}$, where all the background-field-dependent factors are contained in the tensor $\mathcal{T}$. If all eigenvalues of $\mathcal{T}$ are negative, $B<0$ for any polarization. If there is one positive eigenvalue, then it is possible to have $B>0$. If all eigenvalues are positive, $B>0$ for any polarization vector. In Fig. 13 we plot the highest and the lowest eigenvalues of $\mathcal{T}$ before,

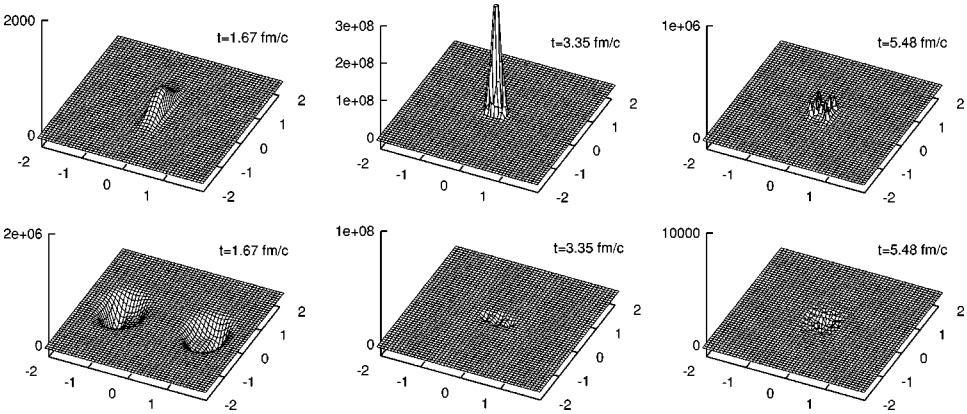

FIG. 13. The highest (top row) and the lowest (bottom row) eigenvalue of the tensor $\mathcal{T}$ at selected moments during annihilation. The unit for the eigenvalues is c^2/fm^4. Note the large differences in the vertical scales. We plot the quantities in the xy plane. The x axis is the direction closer to horizontal. The length on the axes is measured in fm.

during, and after the violent oscillation regime. This illustrates that during free propagation the negative eigenvalues dominate, while during the violent regime, the eigenvalues and also B become very large in absolute value, and the positive eigenvalues dominate. Towards the end of the process, the $B>0$ regime lingers close to the center but is not present in the outgoing radiation. In Fig. 14 we plot the absolute values of the largest and lowest eigenvalues of $\mathcal{T}$ in the whole simulation box as a function of time. The moment of half-annihilation (B) marks a significant increase in the magnitude of the positive eigenvalues, which dominate in the center region through the remainder of the calculation.

In summary, the equations of motion allow in principle for the appearance of exponentially growing perturbations. The conditions for this are rather specific. We are able to show that such conditions accompany the violent, fast-varying regime that follows the unwinding and persist until the outgoing radiation phase. However, we cannot establish a clear, causal connection between the $B>0$ regime and the fluctuations.

V. SINGULAR BEHAVIOR

The source of the persistent small oscillations is the fast-varying behavior that follows the point of half-annihilation.

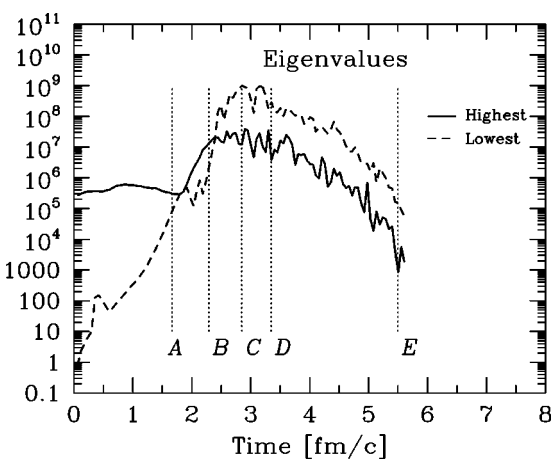

FIG. 14. The absolute values of the lowest (usually negative) and highest (usually positive) eigenvalue of the tensor $\mathcal{T}$ overall during annihilation, in c^2/fm^4. We associate the presence of large positive eigenvalues of $\mathcal{T}$ with instability against perturbations.

The fields at this point and shortly afterwards are singular, or close to that. This is the single most prominent feature of the head-on annihilation process. The few off-center calculations we performed show very similar features.

Our choice of grooming [8] allows a smooth unwinding of the pion field, without any singularity or discontinuity involved. However, it appears that the radial dependence of the field components becomes singular as a result of the dynamics, in the $x=0$ plane close to the moment of half-annihilation. This is the underlying feature that generates the large energy densities in the center seen in Fig. 5. Below we describe this in more detail.

The head-on annihilation process has axial symmetry. In this case, the four ''Cartesian'' components of the pion field are of the form

$$\Psi_0(x,y,z,t)=f(x,\rho,t):\Psi_1(x,y,z,t)=g(x,\rho,t),$$

$$\Psi_2(x,y,z,t)=\frac{y}{\rho}h(x,\rho,t):\Psi_3(x,y,z,t)=\frac{z}{\rho}h(x,\rho,t), \tag{35}$$

where $\rho=\sqrt{y^2+z^2}$ and the chiral constraint is $f^2+g^2+h^2=1$. The components of ω_μ have a similar dependence. The three components of Ψ have additional symmetry constraints; namely, they are all even functions of x. The radial dependence at $\rho\to 0$ inherits the symmetry properties of Ψ, Ψ_0 and Ψ_1 being even functions of y and z while $\Psi_2(-y)=-\Psi_2(y)$ and $\Psi_3(-z)=-\Psi_3(z)$. Therefore f and g are

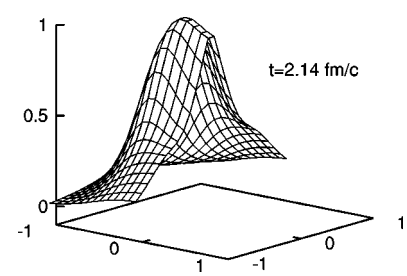

FIG. 15. Pion field $(1-\Psi_0)$ close to half-annihilation. Extrapolating the field to the center would result in a discontinuity in the derivative. The fields are shown in the xy plane. The x axis is the direction closer to horizontal. The length on the axes is measured in fm. The quantity we plot is dimensionless.

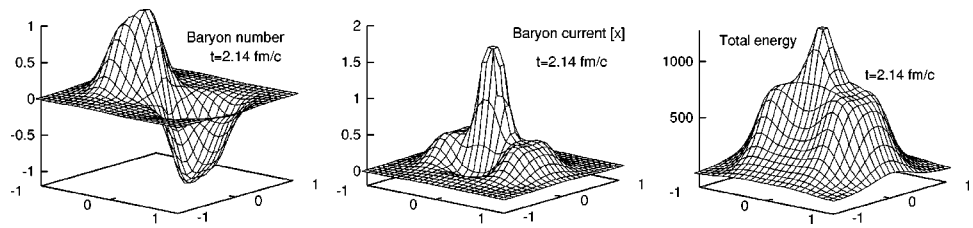

FIG. 16. The baryon number density (in fm^{-3}), the x component of the baryon current density (in c/fm^3), and the energy density (in $\mathrm{MeV/fm}^3$) close to the point of half-annihilation. The fields are shown in the xy plane. The x axis is the direction closer to horizontal. The length on the axes is measured in fm.

''even'' and h is and ''odd'' function of ρ, in the sense that $h_{|\rho=0}=0$ and $\partial_\rho f_{|\rho=0}=\partial_\rho g_{|\rho=0}=0$ when the respective functions are continuous.

Let us consider the $\rho=0$ axis, where only f and g can be nonzero. At $x=\pm\infty$, in free space, we have $f=1$. As one passes through a Skyrmion, the two components ''rotate,'' so that in the center of the Skyrmion we have $f=1$. Similarly, if we choose to move through the ρ direction through the center of the same Skyrmion, the g component would have to vanish by symmetry and the rotation would happen in the fh plane.

The moment of half-annihilation corresponds to the situation when the centers of the Skyrmion and the anti-Skyrmion coincide, i.e., $f=-1$ at $x=0$. Now let us consider the radial dependence in the $x=0$ plane at this moment. At $\rho=0$ we have $f=-1$, $g=0$, and $h=0$. At $\rho=\infty$ we have again $f=1$, $g=0$, $h=0$. In this case, however, the rotation happens involving mostly the f and the h components. At least close to $\rho=0$, g must be much smaller than h, since its first ρ derivative must vanish.

In Fig. 15 we plot $[1-\Psi^0(x,y)]/2=(1-f)/2$, at a moment close to half-annihilation. The field at the center point is close to $f=-1$. As we move outwards along the y (radial) axis, $1-f$ decreases. Notice that the variation of f is concentrated for the most part in a small region around $\rho=0$. In apparent contradiction with the requirement that $f(y)$ should be an even function (hence, $\partial_y f=0$ at $y=0$), $\partial_\rho f=\partial_y f$ increases in magnitude as $y\to 0$. The ρ dependence of f in Fig. 15 is well approximated by a ρ^α with $\alpha=0.2$–0.3. The energy density and the baryon current are both determined by the first derivatives of Ψ^A. The effect is more dramatic in terms of these quantities.

In Fig. 16 we plot the baryon number density, the x component of the baryon current density, and the energy density in the xy plane. The baryon current is concentrated in a very narrow region in the $x=0$ plane, and the energy density has a steep peak that will grow dramatically during the fast-varying regime. We wish to point out that this situation occurs at half-annihilation, just *before* the messy part of the annihilation process. It seems very plausible that this quasi-singular configuration is the ultimate source of the turbulence that follows. Because of the presence of this feature we have been forced to place our grid points so that the symmetry center falls halfway between them in all directions, in order to avoid having to deal with infinite derivatives. We most likely miss the exact moment of the overturn ($f=1$ at $x=\rho=0$). Hence we cannot tell whether the $\alpha\to 0$ limit is achieved [this implies that $f(\rho)$ is a Heaviside function and the baryon current is a delta function, i.e., is all concentrated in the center]. What is clear is that as the overturn is approached the baryon current concentrates more and more in the center, and that close to that moment, the dependence of the field components is consistent with a small power behavior, which in itself leads to infinite derivatives, hence locally infinite energy density.

A precise understanding of the singular phenomenon described above requires a more focused investigation. At this stage we have a qualitative explanation. Recall that our ω field, apart from its mass, is an Abelian gauge field similar to the electromagnetic field. It couples to the respective components of the baryon current $\mathcal{B}$ which, in axial geometry, has only three independent components: the baryon density, the x component, and a radial component. The ω field mediated all interactions in our model. Solitons in the pure nonlinear sigma model collapse because their energy scales as the first power of their linear size. The omega field couples to the baryon (winding number) density. The fact that this stabilizes the Skyrmions against collapse may be interpreted as a consequence of electrostatic repulsion of the baryon charge mediated by the (omega) electric field.

The annihilation process consists of the flow of charges of opposite signs towards the center plane ($x=0$ in our notation), i.e., the presence of a large B^1 component. The fact that the fields vary fast in the center plane means that the baryon current is concentrated in the center or vice versa.[6] The baryon current is very large in the center and is pushed into a small cross section in analogy with the electromagnetic ''pinch'' effect encountered in plasmas. This is a consequence of the attractive interaction between parallel electric currents. This effect competes with the electrostatic repulsion of the charge density. The static charge density must vanish in the center plane, by symmetry (actually, all derivatives of the pion fields with respect to x are zero by symmetry). Therefore here the pinch effect is the strongest. At the time of half-annihilation there is a further depletion of static charge from the $x=0$ region, which would explain why the pinch effect occurs first at or close half-annihilation.

[6]For instance, if the f component behaves like a Heaviside function, then the baryon current is proportional to a delta function as can be seen from its expression which contains only ρ and t derivatives.

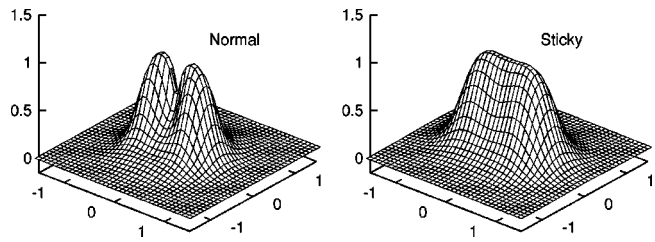

FIG. 17. One component of the pion field $(1-\Psi^0)$ close to half-annihilation, during the true annihilation process and during a calculation where the kinetic energy is periodically depleted by setting time derivatives to zero. The second plot shows no pinching in the middle, indicating that the presence of a baryon current is necessary in order to have a pinch. The fields are shown in the xy plane. The x axis is the direction closer to horizontal. The length on the axes is measured in fm. The quantity we plot is dimensionless.

To test whether we indeed are looking at an electromagnetic effect, we performed a ''sticky slope'' calculation, in which we periodically set the time derivatives of the pion field, as well as the magnetic fields, to zero. This also cancels the baryon current, but not the baryon charge, and the annihilation proceeds ''quasistatically.'' We followed this process to the points where the baryon number in one half-space was 0.55. In Fig. 17 we plot $1-\Psi^0$ at this moment in the sticky slope calculation and, for comparison, the configuration with the same baryon number in a calculation with the same parameters which proceeds normally. The pinching all but disappears in the ''quasistatic'' calculation. This observation is consistent with the contention that the baryon current is responsible for the pinching, since in the sticky slope case there is no current, and as a result the pinching is absent as well.

While the electromagnetic effects offer a qualitative explanation, one would like to have an approach that leads to quantitative understanding, perhaps allowing for an analytical description of the singular part. Furthermore, one may ask the question whether this effect is specific to the omega-stabilized model or is a general feature of dynamically stabilized solitons.

VI. CONCLUSION AND OUTLOOK

We have studied the classical process of annihilation of a Skyrmion and an anti-Skyrmion, in a nonlinear sigma model Lagrangian which couples the SU(2) winding number to a vector field (ω). This coupling stabilizes the Skyrmion without some of the short-wavelength problems inherent in the usual fourth-order Skyrme term. Our ultimate goal is to relate classical annihilation to the physical process of nucleon-antinucleon annihilation. In this paper our goal in more modest. It is to show, for the first time, that annihilation in the classical model can be followed numerically from the initial state of separated Skyrmion and anti-Skyrmion to the final state of outgoing pion and omega radiation. We do encounter some violent behavior in our calculation, but it seems to be tamer than the fatal fluctuations previously encountered in Skyrmion annihilation calculations [7,8]. We are able to follow the calculations from beginning to end with results that are robust and independent of the details of the turbulent behavior.

In this first attempt we only calculate Skyrmion anti-Skyrmion annihilation for head-on collisions and only in the most attractive grooming. Our numerical code permits other initial configurations and we plan to come back to them. We find that annihilation happens very rapidly and is accompanied by a sharp (singular) concentration of the energy density and baryon current. This causes short-wavelength, noisy oscillations but we are able to integrate through them. We find a burst of pion and omega radiation peaked in a cone at 45° with respect to the incident direction. We find turbulent behavior but the calculated outgoing meson field radiation carries the total incident energy to within 8%. We show analytically that our equations of motion allow for a regime which is unstable with respect to the appearance of exponentially increasing (in time) perturbations. However, these conditions are met only in a spatially and temporally limited part of the system under study. This is one possible reason that the instability does not compromise the simulation. We find that the singular concentration of baryon current associated with annihilation is analogous to the pinch effect in electromagnetism. Our theory with a vector field coupled to the current is like electromagnetism, but with a mass. We are studying ways to exploit, analytically, the nature of the singularity to control its contribution. It would be interesting to study whether similar singular behavior involving a peaked baryon current occurs in theories such as the standard Skyrme model, where there is no relation to electromagnetism.

In the future we plan to study Skyrmion–anti-Skyrmion collisions that are not head on and to calculate for other groomings and incident energies. From this we will develop results that can be used to extract predictions for nucleon-antinucleon physics. We also plan to study the singularities we encountered to see if their analytic form can be exploited. It is sometimes the case that in the vicinity of singular behavior one can make precise, analytic statements about solutions to problems that can otherwise only be addressed numerically. It will be interesting to see if that is the case here and to examine how general that approach is. Thus our results suggest ample opportunities for further work both in nucleon annihilation physics and in mathematical physics.

ACKNOWLEDGMENTS

This work was supported in part by a grant from the U.S. National Science Foundation. The calculations have been performed mostly on the National Scalable Cluster Center at the University of Pennsylvania. We are grateful to R. Hollebeek for his continued support. We also thank the Eniac 2000 group for allowing us to use their resources for part of this work. We thank Randy Kamien, Pavlos Protopapas, Krishna Rajagopal, Folkert Tangerman, and Jac Verbaarschot for many useful discussions.

APPENDIX: NUMERICAL METHOD

Here we describe in more detail the numerical algorithm used in the main calculation, which uses the Cartesian com-

ponents Ψ to parametrize the pion field. We use a leapfrog algorithm, based on the equations of motion (17). The time derivatives of the Ψ components as well as the electric field $\mathcal{E}$ and the time derivatives of the ω_k components are defined at half-time steps. The spatial derivatives are calculated as simple centered differences. The discretized equations of motion are written using centered differences in time. For example, equations of the form $\{dv/dt=f(x,v);dx/dt=v\}$ are discretized as

$$\frac{v^{t+1/2}-v^{t-1/2}}{\Delta t}=f\left(x^t,\frac{v^{t+1/2}+v^{t-1/2}}{2}\right)$$

$$\frac{x^{t+1}-x^t}{\Delta t}=v^{t+1/2}. \tag{A1}$$

The initial condition is propagated forward in time by solving the implicit equations for the velocities at $t+1/2$ and the fields at t.

The continuum equations of motion formally preserve the chiral condition $\boldsymbol{\Psi}\cdot\boldsymbol{\Psi}=1$. We ensure this by normalizing the updated Ψ and also using the condition $\dot{\boldsymbol{\Psi}}\cdot\boldsymbol{\Psi}=0$ which is realized at the discretized level by enforcing $\boldsymbol{\Psi}^t\cdot(\dot{\boldsymbol{\Psi}}^{t+1/2}+\dot{\boldsymbol{\Psi}}^{t-1/2})=0$. Some additional precautions are taken to wrap the variation vector $\dot{\boldsymbol{\Psi}}\Delta t$ around the unit sphere. Also, we found that locally performing a rotation in SU(2) space so that the current $\boldsymbol{\Psi}$ is close to the equator on the unit sphere (and modifying the equations of motion—in particular, the pion mass term—accordingly) enhances the stability of the calculation. This rotation in similar to the one we perform in the π scheme. For details of that scheme (the algorithm is very similar) we refer to [9].

In addition to the regular points in the simulation box we also have a layer of ten points in each spatial direction on the exterior walls. The spacing of these points increases from the regular spacing up to several times that. The fields at the final points are set to zero. This simulates an absorbing boundary, which was tested and worked satisfactorily in our scattering paper [9]. However, those calculations were performed with larger simulation boxes. In the scaling runs we refer to in this paper, we do see some effect of the walls for times larger than 5 fm/c.

[1] T. H. R. Skyrme, Proc. R. Soc. London **262**, 237 (1961); Nucl. Phys. **31**, 556 (1962).

[2] E. Witten, Nucl. Phys. **160**, 57 (1979).

[3] For reviews on the subject of Skyrmions, see I. Zahed and G. E. Brown, Phys. Rep. **142**, 1 (1986); T. Gisinger and M. B. Paranjape, *ibid.* **306**, 109 (1998).

[4] Y. Lu, P. Protopapas, and R. D. Amado, Phys. Rev. C **57**, 1983 (1998); Y. Lu and R. D. Amado, *ibid.* **54**, 1566 (1996).

[5] Y. Lu and R. D. Amado, Phys. Rev. C **52**, 2158 (1995); B. Shao and R. D. Amado, *ibid.* **50**, 1787 (1994).

[6] J. J. M. Verbaarschot, T. S. Walhout, J. Wambach, and H. W. Wyld, Nucl. Phys. **A461**, 603 (1987); J. J. M. Verbaarschot, Phys. Lett. B **195**, 235 (1987).

[7] W. Y. Crutchfield and J. B. Bell, J. Comput. Phys. **110**, 234 (1994).

[8] H. M. Sommermann, R. Seki, S. Larson, and S. E. Koonin, Phys. Rev. D **45**, 4303 (1992).

[9] R. D. Amado, M. Á. Halász, and P. Protopapas, Phys. Rev. D **61**, 074022 (2000).

[10] U. G. Meissner and I. Zahed, Phys. Rev. Lett. **56**, 1035 (1986).

[11] G. S. Adkins and C. R. Nappi, Phys. Lett. **137B**, 251 (1984).

[12] D. A. Dwyer and K. Rajagopal, Phys. Rev. D **62**, 105028 (2000).

[13] A. E. Allder, S. E. Koonin, R. Seki, and H. M. Sommerman, Phys. Rev. Lett. **59**, 2836 (1987).

[14] B. Piette, P. M. Sutcliffe, and W. J. Zakrzewski, Int. J. Mod. Phys. C **3**, 637 (1992).

[15] B. M. Piette, B. J. Schroers, and W. J. Zakrzewski, Nucl. Phys. **B439**, 205 (1995); A. Kudryavtsev, B. Piette, and W. J. Zakrzewski, Phys. Lett. A **180**, 119 (1993).